metals

MDPI

Article

Testing the Applicability of ^{119}Sn Mössbauer Spectroscopy for the Internal Stress Study in Ternary and Co-Doped Ni-Mn-Sn Metamagnetic Alloys

I. Unzueta [1,*], J. López-García [2,3], V. Sánchez-Alarcos [3,4], V. Recarte [3,4], J. I. Pérez-Landazábal [3,4], J. A. Rodríguez-Velamazán [2], J. S. Garitaonandia [5], J. A. García [5] and F. Plazaola [6]

1 Department of Applied Mathematics, University of the Basque Country (UPV/EHU), Torres Quevedo Ingeniaria Plaza 1, 48013 Bilbao, Spain
2 Institut Laue Langevin, 71, Avenue des Martyrs, CEDEX, 38042 Grenoble, France; javier.lopezg@unavarra.es (J.L.-G.); velamazan@ill.eu (J.A.R.-V.)
3 Departamento de Ciencias, Public University of Navarra (UPNA), 31006 Pamplona, Spain; vicente.sanchez@unavarra.es (V.S.-A.); recarte@unavarra.es (V.R.); ipzlanda@unavarra.es (J.I.P.-L.)
4 Institute for Advanced Materials and Mathematics INAMAT^2, Universidad Pública de Navarra, 31006 Pamplona, Spain
5 Fisika Aplikatua II Saila, Euskal Herriko Unibersitatea UPV/EHU, 48940 Leioa, Spain; js.garitaonandia@ehu.eus (J.S.G.); joseangel.garcia@ehu.eus (J.A.G.)
6 Elektrizitate eta Elektronika Saila, Euskal Herriko Unibersitatea UPV/EHU, 48940 Leioa, Spain; fernando.plazaola@ehu.es
* Correspondence: iraultza.unzueta@ehu.eus; Tel.: +34-946014297

Abstract: The influence of both the Co addition and the internal stress on the atomic level magnetism is comparatively studied in $Ni_{50}Mn_{37}Sn_{13}$ and $Ni_{45}Mn_{38}Sn_{13}Co_4$ alloys by magnetic measurements and ^{119}Sn Mössbauer spectroscopy. The results show that the saturation magnetization and the hyperfine field follow the same temperature trend. The internal stress state is investigated by subjecting the samples to milling and annealing treatments, and tracking the singlet component revealed by ^{119}Sn Mössbauer spectroscopy. Contrary to what was expected, in the Co-doped Ni-Mn-Sn sample the singlet component can be resolved between the milled and annealed states in both martensite and austenite phases. Therefore, the results demonstrate the feasibility of tracking the singlet component upon the structural recovery in Co-doped Ni-Mn-Sn alloys in a much wider range than in ternary alloys. In addition, it is concluded that the transferred dipolar field at Sn from the neighbor magnetic atoms depends very strongly on the stress field and on the microstructural order surrounding Sn atoms. The observed sensitivity of Sn Mössbauer probe atoms to slight microstructural distortions make ^{119}Sn a powerful technique for the characterization of the stress present in Sn containing metamagnetic shape memory alloys.

Keywords: metamagnetic shape memory alloys; structural defects; ^{119}Sn Mössbauer spectroscopy; internal stress

Citation: Unzueta, I.; López-García, J.; Sánchez-Alarcos, V.; Recarte, V.; Pérez-Landazábal, J.I.; Rodríguez-Velamazán, J.A.; Garitaonandia, J.S.; García, J.A.; Plazaola, F. Testing the Applicability of ^{119}Sn Mössbauer Spectroscopy for the Internal Stress Study in Ternary and Co-Doped Ni-Mn-Sn Metamagnetic Alloys. *Metals* **2021**, *11*, 450. https://doi.org/10.3390/met11030450

Academic Editors: Jiro Kitagawa and Mikhaïl A. Lebyodkin

Received: 31 January 2021
Accepted: 28 February 2021
Published: 9 March 2021

1. Introduction

Ni-Mn-based Heusler alloys have been extensively studied during recent decades due to the multifunctional properties they exhibit such as giant magnetoresistance [1], magnetocaloric effect [2] and shape memory effect [3]. Their multifunctional properties are linked to the occurrence of the martensitic transformation (MT), which is a first order phase transition between a cubic austenite phase and a less-symmetric martensite one. Among the Ni-Mn-based Heusler alloys family, the so-called metamagnetic shape memory alloys Ni-Mn-Z (Z = In, Sn, Sb) have attracted considerable interest, in which, unlike the ferromagnetic shape memory alloys, the MT occurs between ferromagnetic austenite and weak magnetic martensite phases. The magnetization difference (ΔM) between the

two phases gives rise to additional multifunctional properties such as the magnetic field-induced shape memory effect [4] and the inverse magnetocaloric effect [5,6].

To enhance the metamagnetic character of these alloys, the addition of cobalt (Co) has been found to be an effective way. In both Ni-Mn-In and Ni-Mn-Sn alloys, Co doping decreases the MT temperature while increases considerably the Curie temperature T_c [7]. Additionally, by adding Co, the magnetism of the austenite phase increases significantly while the magnetism of the martensite phase decreases relative to that of the ternary counterpart. As a result, the ΔM increases. This effect is especially notorious in Ni-Mn-In-Co alloys, in which an almost non-magnetic martensite phase is obtained showing enhanced magnetocaloric properties [8]. In Co-doped Ni-Mn-Sn alloys, although ΔM also increases, the obtained metamagnetic character is in general smaller compared to In-based ones. However, Ni-Mn-Sn alloys present a highly stable long-range atomic order structure against thermal treatments, becoming a good candidate for thermocycling involving applications [9].

Despite these promising features, the deficient mechanical properties of bulk samples hinder the development of practical applications. As a result, the use of microparticles is attracting increasing interest as an effective method to overcome the drawbacks of bulk samples [10]. However, in micro- and nano-regime the control of internal stresses and defects becomes crucial to properly tune the desired multifunctional properties [11,12]. During thermal cycling, the retained residual stress degrades the MT, increasing its hysteresis and its irreversibility [13,14]. On the other hand, the presence of defects inhibits the MT and they have a great impact on the ferromagnetic (FM) interactions [15]. Thus, in such regime, the knowledge of the local stress and its characterization acquires a key importance.

In a recent work [16] the effect of the internal stress on the MT in a $Ni_{50}Mn_{35}Sn_{15}$ alloy has been monitored by ^{119}Sn Mössbauer Spectroscopy (^{119}Sn-MS). It has been shown that the non-magnetic (singlet) component revealed by ^{119}Sn-MS is directly related to the stressed regions. On top of that, the singlet component and the recovery of the MT evolve mutually. Thus, by means of ^{119}Sn-MS it is possible to track the evolution of the MT upon microstructural recovery. However, the main drawback of the approach resides on the fact that a proper characterization could only be performed on alloys in which the non-magnetic component related to the stress is clearly differentiated in the Mössbauer spectra. Indeed, in Ni-Mn-Sn systems with a low magnetic hyperfine field (B_{hf}), this characterization might not be possible.

On the other hand, the area of the non-magnetic component is directly related with the presence of the anti-phase boundaries (APBs), where the Mn atoms couple antiferromagnetically (AF) in an otherwise FM material [17,18]. Due to the AF coupling between Mn atoms across APBs, the hyperfine field felt by Sn nucleus is zero, giving rise to the non-magnetic singlet component in ^{119}Sn Mössbauer spectra [16]. As a result, the gradual fade-out that the singlet component exhibits upon annealing has been explained in terms of the gradual recovery that the Mn-Mn coupling experiences during the transition from AF to FM state. In this context, V. Sánchez-Alarcos et al. [12] have recently shown that the presence of Co in Ni sites makes the coupling between Mn atoms to be always FM in the austenite phase, and AF in the martensite phase, irrespectively of the presence of defects or internal stresses. Thus, in Co-doped Ni-Mn-Sn samples, although the magnetic component increases as compared to the ternary alloy, the method described in Ref. [16] may have some limitations due to the absence of Mn-Mn magnetic coupling change between the milled and annealed states in both austenite and martensite phases.

This work is devoted to elucidating the applicability of the approach developed in Ref. [16] for other Ni-Mn-Sn alloys, and to investigate, whether Co addition enables a better identification of the stress-related non-magnetic component revealed by ^{119}Sn-MS. The results show that for the $Ni_{50}Mn_{37}Sn_{13}$ ternary alloy, the method is only feasible within a certain temperature range, where the areas of the singlet and sextet components enable the clear distinction between them. In the case of $Ni_{45}Mn_{38}Sn_{13}Co_4$ sample, it is possible to properly identify the singlet component due to the enhanced magnetism of the alloy.

In addition, the results show that at 160 K, the singlet component is detectable in the Mössbauer spectra of the ternary alloy; however, at 64 K, the singlet fades out even in the milled state, where in principle, the AF coupling across the APBs should still contribute with a singlet to the ^{119}Sn Mössbauer spectra. In the Co-doped Ni-Mn-Sn sample, contrary to what was expected, the singlet component exhibits a clear evolution upon annealing in both austenite and martensite phases, thus enabling the tracking of the singlet component during the microstructural recovery.

2. Experimental

Ni-Mn-Sn and Ni-Mn-Sn-Co polycrystalline ingots were synthesized from high purity elements by arc-melting method under protective argon atmosphere, and re-melted up to eight times to ensure homogeneity. Afterwards, for a complete homogenization of the alloys, the ingots were annealed for 24 hours at 1173 K. The samples were cut using a low-speed diamond saw and pieces from the central part were taken for the initial characterization. The measured composition, checked by EDX, were $Ni_{50}Mn_{37}Sn_{13}$ and $Ni_{45}Mn_{38}Sn_{13}Co_4$. The magnetic measurements were performed using a QD MPMS XL-7SQUID magnetometer, revealing a similar T_c and MT temperature for $Ni_{50}Mn_{37}Sn_{13}$, and a MT temperature $\approx$ 200 K for $Ni_{45}Mn_{38}Sn_{13}Co_4$ with a T_c = 390 K [19,20]. Due to the lack of resolution of the magnetic measurements for the concurrent characterization of T_c and the MT temperature, the MT temperature of the ternary alloy has been characterized in greater detail by using a TA Q100 Differential Scanning Calorimeter (DSC) at a heating/cooling rate of 10 K/min, revealing a MT temperature of 320 K. To study both austenite and martensite phases, Mössbauer spectra were obtained using a $Ba^{119m}SnO_3$ source in a transmission setup at normalized temperatures of T/T_c = 0.9, 0.5 and 0.2, corresponding to; 285 K, 160 K and 64 K in the $Ni_{50}Mn_{37}Sn_{13}$ sample and 351 K, 195 K and 78 K in the $Ni_{45}Mn_{38}Sn_{13}Co_4$ sample one. Spectra were fitted using NORMOS [21] program and isomer shift values are referenced to $CaSnO_3$ at room temperature.

With the aim of inducing stress, the two ingots have been mechanically crushed using an agate mortar, following the approach of Ref. [16]. To analyze the atomic scale magnetism upon post-milling annealing, from each milled sample some powder was taken apart and annealed at 873 K for 5 minutes. The samples were labeled as Sn13M, Sn13AN, Sn13CoM and Sn13CoAN, where Sn13 and Sn13Co refer to the composition, and M and AN stand for the milled and annealed state, respectively. The atomic structure of the powdered samples was analyzed by powder neutron diffraction at the Institute Laue-Langevin in Grenoble (France), using the D2B instrument (λ = 1.59 Å). The diffraction data has been refined using the FullProf package [22].

3. Results

Figure 1 shows the neutron diffraction spectra for the milled and annealed $Ni_{50}Mn_{37}Sn_{13}$ and $Ni_{45}Mn_{38}Sn_{13}Co_4$ samples. Due to the fact that the structure of the austenite phase is better resolved than that of martensite during the Rietveld refinement, the long-range atomic order has been analyzed in the austenite phase ($Fm\bar{3}m$). Thus, the spectra were taken at 420 K and 300 K (above their MT temperature) for the ternary and quaternary alloy, respectively. The diffractograms show the same relative intensities in the reflection peaks in both milled and annealed samples, denoting the lack of atomic disorder between the two different states of the same sample. This fact is corroborated by the occupancy values obtained from the Rietveld refinement shown in Table 1. Moreover, the milled and annealed samples have similar lattice parameters: 5.9851(1) Å and 5.9823(3) Å for $Ni_{50}Mn_{37}Sn_{13}$ and 5.979 Å and 5.984 Å for $Ni_{45}Mn_{38}Sn_{13}Co_4$, respectively. Thus, it can be concluded that no atomic disorder has been brought during the milling and subsequent annealing of the studied samples, in agreement with previous reports [16,23]. The only observable feature is a slight narrowing of the width of diffractions peaks, pointing out relaxation/recovery processes.

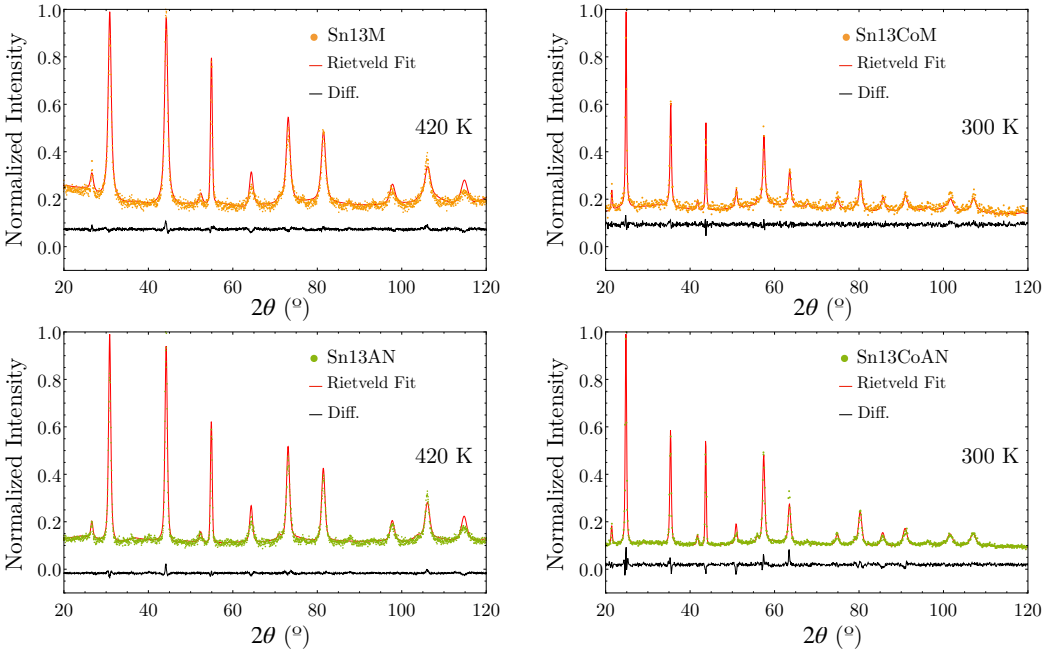

Figure 1. Neutron Diffraction pattern for the milled and annealed Sn13 and Sn13Co samples. The measurements were taken at 420 and 300 K, respectively, to study the long-range atomic order of the austenite phase ($Fm\bar{3}m$). The diffraction data corroborates the lack of atomic disorder for the milled as well as for the annealed samples.

Table 1. Occupancies for $4a$ $(0,0,0)$, $4b$ $(1/2,1/2,1/2)$ and $8c$ $(1/4,1/4,1/4)$ positions of the milled and annealed $Ni_{50}Mn_{37}Sn_{13}$ and $Ni_{45}Mn_{38}Sn_{13}Co_4$ samples obtained from the Rietveld refinement at 420 K and 300 K, respectively. The obtained values indicate the same atomic structure in the milled and annealed sample of each composition.

	$Ni_{50}Mn_{37}Sn_{13}$			**$Ni_{45}Mn_{38}Sn_{13}Co_4$**		
	Site 4*a*	**Site 4*b***	**Site 8*c***	**Site 4*a***	**Site 4*b***	**Site 8*c***
M	Mn 0.82(1) Ni 0.08(3) Sn 0.10(6)	Mn 0.47(1) Ni 0.13(3) Sn 0.40(6)	Mn 0.09(6) Ni 0.90(2) Sn 0.01(3)	Mn 0.942(19) Ni, Co (—) Sn 0.059(17)	Mn 0.5353(16) Ni, Co (—) Sn 0.4846(9)	Ni 1.80(14) Co 0.18(10) Sn, Mn (—)
AN	Mn 0.83(1) Ni 0.09(3) Sn 0.08(6)	Mn 0.45(1) Ni 0.13(3) Sn 0.43(6)	Mn 0.10(5) Ni 0.89(2) Sn 0.01(3)	Mn 0.9501(15) Ni, Co (—) Sn 0.057(10)	Mn 0.537(11) Ni, Co (—) Sn 0.471(10)	Ni 1.81(16) Co 0.19(9) Sn, Mn (—)

To correlate the macroscopic magnetism with that of the atomic level, the magnetization of the samples (above and below the MT) have been measured. Figure 2 shows the magnetic field-dependent magnetization measurements ($M(H)$ curves) performed for milled and annealed $Ni_{50}Mn_{37}Sn_{13}$ and $Ni_{45}Mn_{38}Sn_{13}Co_4$ alloys. The effect of the Co addition in the magnetism is clearly observed. Although in the Sn13AN sample the maximum saturation magnetization (M_s) is ≈30 Am^2/kg, the addition of Co increases it up to ≈90 Am^2/kg. On the other hand, the M_s of the ternary alloy increases along with temperature decrease. However, in $Ni_{45}Mn_{38}Sn_{13}Co_4$ sample M_S increases until the MT takes place (≈200 K), below which M_s decreases. $M(H)$ curves also show a significant increase of M_s after annealing, pointing out the structural recovery taking place upon annealing, which reinforces the macroscopic magnetism.

In addition, Figure 2 also shows $M(T)$ and DSC measurements. They reveal similar T_c for the milled and annealed Sn13 and Sn13Co samples. Given the high sensitivity of T_c to slight atomic order variations [24,25], the same value of T_c indicates the lack of atomic order differences between the milled and annealed samples. Thus, the observed changes on the macroscopic magnetism must rely on the different internal stress state induced

during milling. Up to now, the magnetic characterization reveals that the macroscopic magnetism of the ternary alloy is smaller than the one of the Co-doped sample, which is greatly affected by the internal stresses induced during milling. Thus, according to the approach in Ref. [16], this effect may also be reflected by ^{119}Sn-MS measurements, which finally could also add a valuable information about the evolution of the MT.

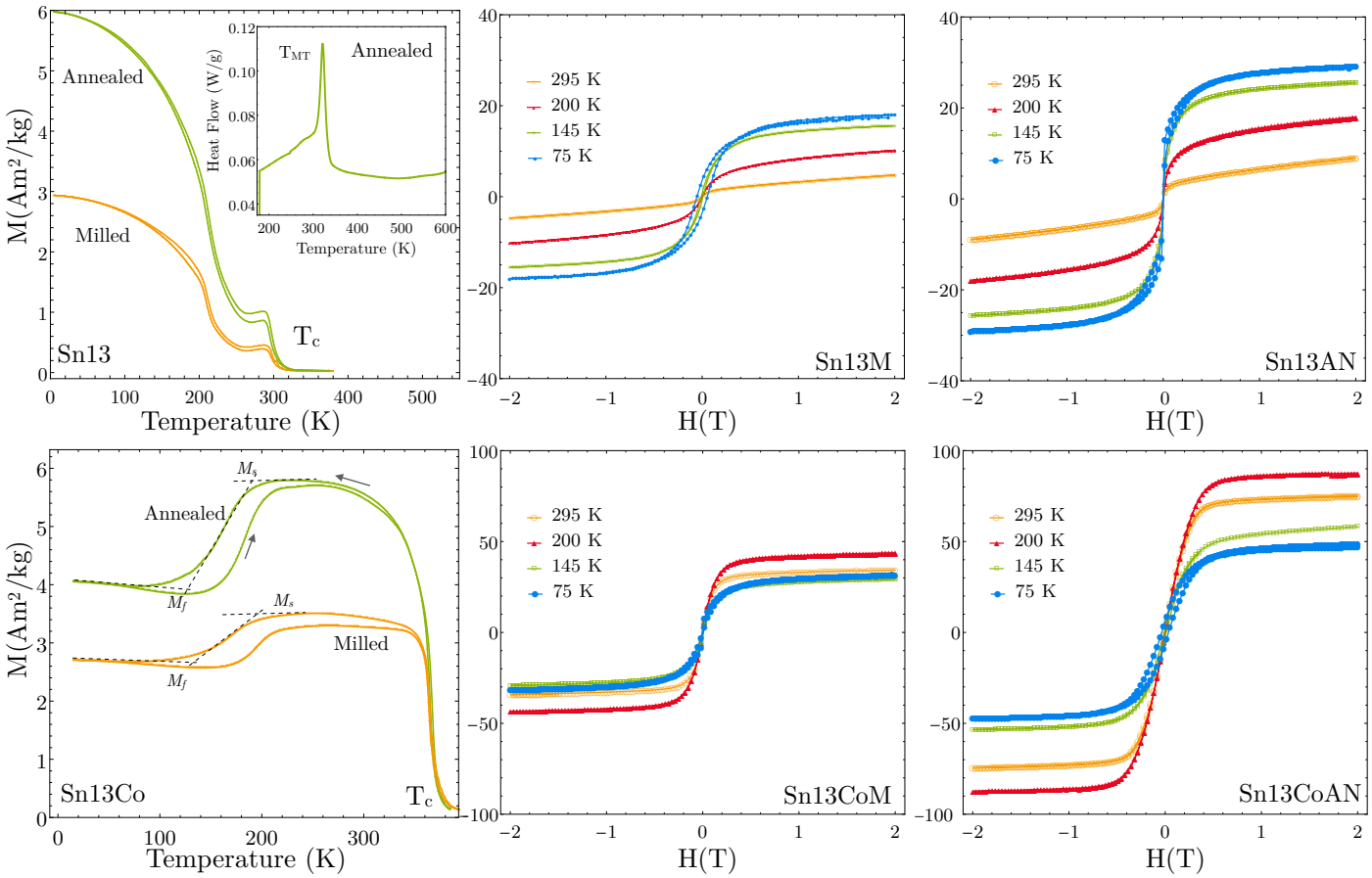

Figure 2. From left to right, $M(T)$ curves and $M(H)$ curves for Sn13M, Sn13AN samples (top row) and for Sn13CoM and Sn13CoAN samples (bottom row) recorded at several temperatures. The inset in Sn13 sample shows the direct martensitic transformation peak (on cooling) of the annealed Sn13 sample. In all the milled samples the magnetization decreases in comparison with their annealed counterparts. Additionally, the Co-doped sample shows a larger M_s value.

The milled and annealed Sn13 and Sn13Co samples have been measured by ^{119}Sn-MS at room temperature, to verify whether the influence of the milling and the subsequent annealing is revealed as in the macroscopic magnetic measurements. Spectra are shown in Figure 3 while the parameters obtained from the fitting are displayed in Table 2. In the case of the ternary alloy, both milled and annealed state exhibit similar features. The annealing of the internal stresses does not affect significantly the features of spectra, and only a small recovery in the magnetic component is observed between Figure 3a,c. In the Sn13Co sample, however, the annealing of the non-magnetic component is clearly quantifiable. Indeed, the Sn13CoAN spectrum does not exhibit the singlet component related to the presence of the internal stress [16].

The different areas of the singlet and magnetic component observed in each $Ni_{50}Mn_{37}Sn_{13}$ and $Ni_{45}Mn_{38}Sn_{13}Co_4$ spectra could be affected by two facts. On the one hand, the ternary alloy is measured in the martensite phase, while the quaternary alloy is measured in the austenite phase. On the other hand, the spectra could also be affected by the different proximity between the measurement temperature and the corresponding T_c. In the ternary alloy the ^{119}Sn-MS measurement temperature is close to its $T_c = 320$ K, and for the Co-doped sample the room temperature is well below its $T_c = 390$ K. Thus,

to properly compare the spectra components, ^{119}Sn-MS measurements have been taken at $T/T_c = 0.9, 0.5$ and 0.2 normalized temperatures. Moreover, within this temperature range, the quaternary alloy has been measured in both austenite and martensite phases, to ascertain the applicability of the approach of Ref. [16].

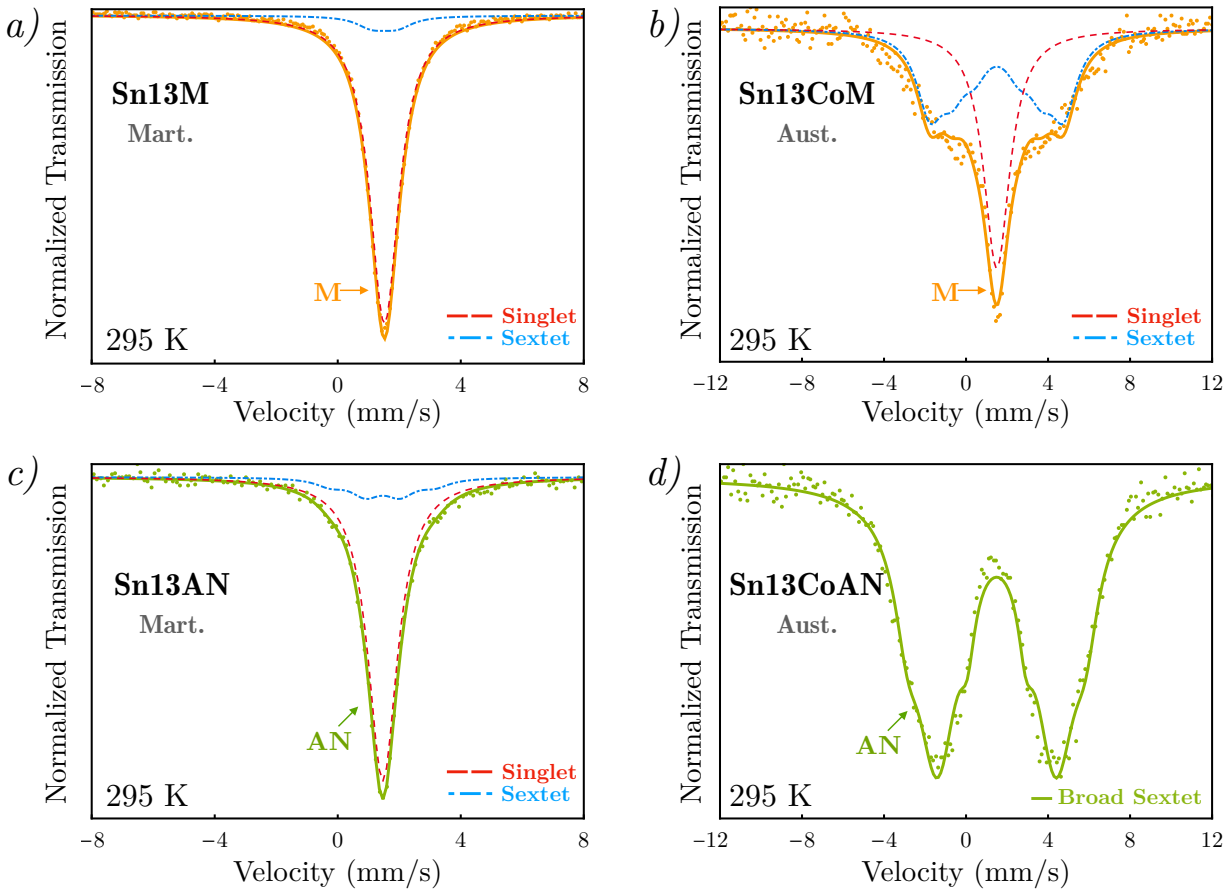

Figure 3. ^{119}Sn Mössbauer spectra for (**a**) Sn13M, (**b**) Sn13CoM, (**c**) Sn13AN and (**d**) Sn13CoAN samples measured at 295 K. The former three spectra have been fitted using a singlet and a magnetic component, while Sn13CoAN spectrum have been fitted using a single magnetic component (broad sextet). *Aust.* and *Mart.* labels refer to austenite and martensite phase, respectively.

Figure 4 shows the ^{119}Sn-MS experimental and fitted spectra for $Ni_{50}Mn_{37}Sn_{13}$ and $Ni_{45}Mn_{38}Sn_{13}Co_4$ samples in both milled and annealed state taken at T/T_c normalized temperatures. It is noteworthy to mention that the MT temperature of the $Ni_{50}Mn_{37}Sn_{13}$ sample is $\approx$ 320 K, while that of $Ni_{45}Mn_{38}Sn_{13}Co_4$ sample is $\approx$ 200 K. This implies that for $Ni_{50}Mn_{37}Sn_{13}$ sample, all spectra have been measured in the martensite phase, while for the quaternary alloy only those measured at 78 K are in the martensite phase (Figure 4i,l). Although for the $Ni_{45}Mn_{38}Sn_{13}Co_4$ sample the MT starts at 200 K, the transformation extends over $\approx$90 K, which implies that on the direct transformation (from austenite to martensite, on cooling) the sample is mostly in the austenite phase at 195 K.

Following the approach of Ref. [16] the fitting of the ^{119}Sn-MS spectra has been carried out as follows: (i) using two discrete components, a singlet and a sextet, with the isomer shift (δ) constrained to be the same for the two subspectra, see Figures 3a–c and 4a,b,d,g–i. (ii) when the spectrum does not exhibit the central non-magnetic component, a fitting attempt has been made using a single broad sextet component, to better capture the magnitude of the hyperfine field (B_{hf}), see Figures 3d and 4c,e,j,k. (iii) when the previous two strategies do not lead to a good fit, an hyperfine field distribution has been used, see Figure 4f,l. The fitting using a broad sextet has been prioritized over the use of hyperfine field distributions because, in the latter, the B_{hf} showed larger variability as a function of the

fitting parameters, while in the fittings where a broad sextet has been used, the magnitude of B_{hf} was less sensitive to those parameters. Despite the lower symmetric structure of the martensite phase in comparison to the austenite one, the quadrupole shift has been considered to be zero in accordance with previous reports [15,26–28]. Although fits with better χ^2 could be obtained, the described fitting procedure turned out to be the one that best captures a coherent evolution of the fitting parameters. These results are collected in Table 2.

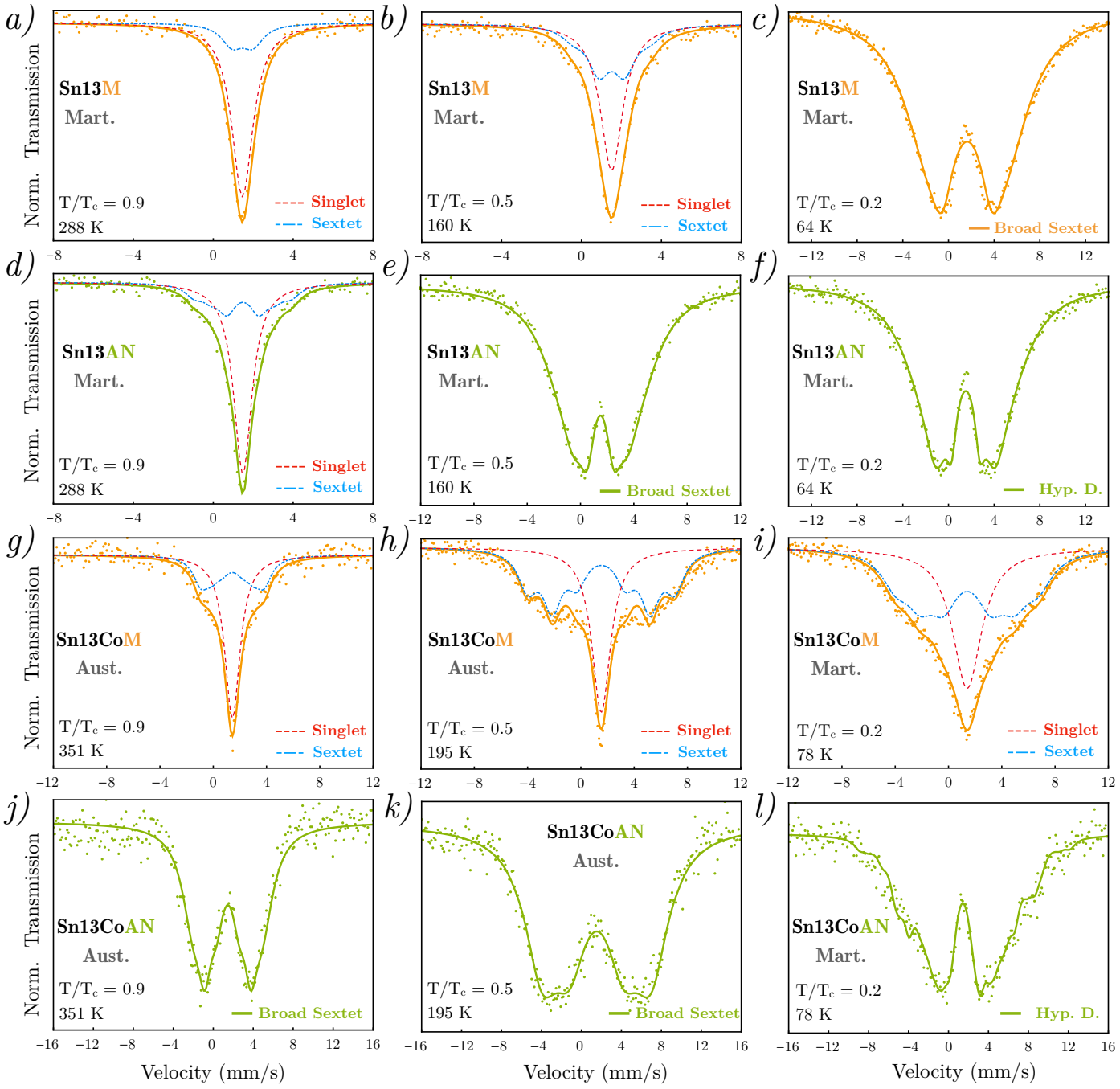

Figure 4. ^{119}Sn Mössbauer spectra for the annealed (AN) and milled (M) state of (**a**–**f**) Sn13 and (**g**–**l**) Sn13Co samples measured at normalized temperatures $T/T_c = 0.9, 0.5$ and 0.2. The fitting has been carried out using two discrete components (singlet and sextet), a broad sextet or using a distribution of hyperfine fields (Hyp. D).

Table 2. The value of $B_{hf}(T)$ magnetic hyperfine field, δ(mm/s) isomer shift, and the A_s(%) area of the singlet (area of the sextet $A_B = 100\% - A_s$) obtained from the fitting for $Ni_{50}Mn_{37}Sn_{13}$ and $Ni_{45}Mn_{38}Sn_{13}Co_4$ alloys in both milled and annealed state at the indicated temperatures. δ has been constrained to be the same for both singlet and sextet subspectra [16].

		$Ni_{50}Mn_{37}Sn_{13}$				$Ni_{45}Mn_{38}Sn_{13}Co_4$			
		295 K	**288 K**	**160 K**	**64 K**	**351 K**	**295 K**	**195 K**	**78 K**
Milled	$B_{hf}(T)$	1.0(5)	1.5(2)	3.9(3)	6.54(2)	4.8(1)	6.56(4)	11.11(7)	10.7(2)
	$\delta(mm/s)$	1.51(1)	1.46(2)	1.50(1)	1.52(1)	1.44(1)	1.497(7)	1.529(9)	1.4(2)
	A_s(%)	93(2)	80(2)	57(4)	(—)	62(2)	45.6(1)	39.9(6)	36(3)
	A_B(%)	7	20	43	100	38	54.4	60.1	64
Annealed	$B_{hf}(T)$	3.55(9)	4.9(1)	6.00(6)	7.8(2)	6.92(5)	7.12(1)	16.5(2)	13.1(5)
	$\delta(mm/s)$	1.5(1)	1.48(2)	1.5(1)	1.51(1)	1.46(1)	1.47(1)	1.52(2)	1.5(3)
	A_s(%)	87(3)	66.9(8)	(—)	(—)	(—)	(—)	(—)	(—)
	A_B(%)	13	33.1	100	100	100	100	100	100

4. Discussion

As shown in Table 2, the fitting process reveals similar values of δ between the corresponding milled and annealed samples at each temperature, which are mostly centered at around 1.5 mm/s. Thus, the isomer shift values of the ^{119}Sn Mössbauer spectra point out that the milled and annealed samples preserve the same atomic order. This parameter is highly sensitive to the chemical disorder in the very close environment of the Mössbauer probe atom (Sn in this case). The lack of variation indicates the absence of atomic disorder [29], which supports the previous hypothesis related to the origin of the observed changes occurring as a consequence of the induced local stress rather than due to different atomic ordering of the milled and annealed samples.

The spectra of Sn13M sample taken at 295 K, 288 K and 160 K (see Figures 3a and 4a,b) exhibit a single central absorption line, which becomes broader at the wings when temperature decreases. This broadening is observed in more detail in the spectra of Sn13AN sample, Figures 3c and 4d, which is related to the sextet contribution. Due to the annealing of the internal stress, the magnetism is recovered, giving rise to a greater magnetic contribution to the spectra. As shown in Table 2, the area of the singlet component decreases from 93% to 87% at 295 K, and from 80% to 67% at 288 K after annealing. At 160 K, the Sn13AN sample does not show the stress-related singlet component, which is completely annealed out during the treatment at 873 K (see Figure 4e). In addition, as shown in Figure 4c,f, at 64 K, neither Sn13M nor Sn13AN exhibits the stress-related singlet component. Although at higher temperatures the singlet is present, at 64 K only a broad magnetic component is observed. At this temperature, the only effect of the annealing is the hyperfine field increase, which raises from ≈6.54 T up to 7.8 T. Taking into account that the singlet component "vanishes" at low temperatures, even in the milled state, it indicates that the approach of Ref. [16] can be only performed within a certain temperature range.

In the case of Sn13CoM milled sample, the stress-related singlet component is clearly identifiable in all spectra (see Figures 3b and 4g–i). On the one hand, the magnetic component is visible even at 351 K, see Figure 4g. The value of B_{hf} increases considerably with respect to that of the ternary alloy, thus enabling a better resolution between the singlet and the sextet component, see Table 2. The area of the magnetic sextet ($A_B = 100\% - A_s$) becomes more and more intense with decreasing temperature. The area A_B increases from 38% at 351 K up to 64% at 78 K. After annealing the milled sample, all Sn13CoAN samples do not exhibit any singlet feature, and the stress-related component is clearly vanished, see Figures 3d and 4j–l. At $T/T_c = 0.2$ (martensite phase) the singlet component of Sn13CoAN shown in Figure 4i,l is annealed too, and the spectra also shows a more resolved magnetic splitting than the Sn13CoM sample. The effect that the annealing induces on the area of both sextet and singlet components is quantifiable over the studied temperature range. Therefore, the feasibility of the approach of Ref. [16] is much better in the $Ni_{45}Mn_{38}Sn_{13}Co_4$

sample than in the ternary alloy. Even in the martensite phase, at $T/T_c = 0.2$, and in contrast to what happened in the case of the ternary $Ni_{50}Mn_{37}Sn_{13}$ sample (compare with Figure 4c,f) it is possible to track the stress-related singlet component, and therefore, the structural recovery taking place upon annealing.

Figure 5 shows the temperature evolution of M_s (a) and B_{hf} (b) of the Sn13 and Sn13Co samples in the milled and annealed states. The M_s of the milled samples is lower than that of the annealed ones. Therefore, the stress induced during the milling decreases the overall magnetization in both $Ni_{50}Mn_{37}Sn_{13}$ and $Ni_{45}Mn_{38}Sn_{13}Co_4$ alloys. This macroscopic magnetization reduction has been previously reported in other Heusler alloys [30,31]. When milling (i.e., cold working), dislocations are induced in the samples, which are accompanied by anti-phase boundaries [32]. In these regions the second nearest neighbor Mn atom couples AF in an otherwise FM material [17]. As a consequence, the total number of Mn atoms contributing to the ferromagnetism decreases, and so does M_s. This reduction is also reflected by ^{119}Sn-MS. As shown in Table 2 and in Figure 5b, the B_{hf} of Sn13M and Sn13CoM samples decreases as compared to their annealed counterparts. In the case of the ternary alloy the qualitative evolution of M_s and the B_{hf} follow a similar decreasing linear trend. As shown in Figure 5a, for Sn13M and Sn13AN samples, M_s decreases monotonically with increasing the temperature, as it happens with B_{hf}. For $Ni_{45}Mn_{38}Sn_{13}Co_4$, in the austenite phase, both B_{hf} and M_s increase as the temperature decreases. However, in the martensite phase, $\lesssim$ 200–195 K, both B_{hf} and M_s decrease with respect to the value at MT. Thus, the B_{hf} also reflects the metamagnetic character and the ΔM between the two phases, which, in turn, lay the ground of the macroscopic magnetic evolution shown in Figures 2 and 5a.

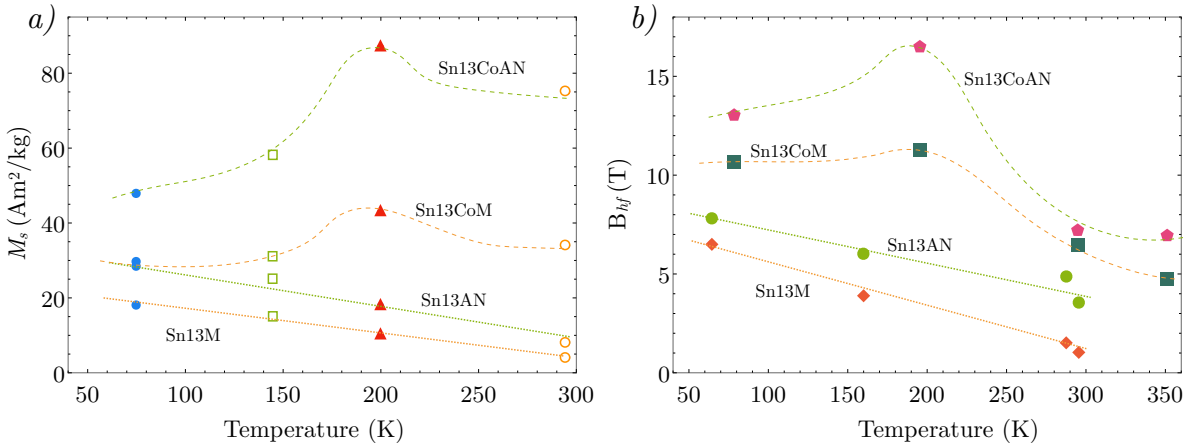

Figure 5. The temperature evolution of the M_s (**a**) and B_{hf} (**b**) of the milled and annealed $Ni_{50}Mn_{37}Sn_{13}$ and $Ni_{45}Mn_{38}Sn_{13}Co_4$ samples. The lines are a guide to the eye.

In this connection, it is interesting to notice the different Mn-Mn coupling detected by neutron diffraction in the martensitic phase between ternary and quaternary alloys in and Ref. [16] and Ref [12], respectively. In the case of $Ni_{50}Mn_{35}Sn_{15}$, the coupling between Mn atoms in 4*a* and 4*b* positions is AF in the milled sample, which becomes FM upon annealing. However, in the case of $Ni_{45}Co_5Mn_{35}Sn_{15}$, the Mn-Mn coupling between 4*a* and 4*b* positions remains always FM/AF in austenite/martensite phases, respectively, for both milled and annealed states. Overall, in Ni-Mn-Sn alloys the ^{119}Sn Mössbauer spectra show magnetic components related to Sn atoms, but Sn atoms do not carry intrinsic magnetic moment. However, a transferred hyperfine field can be induced from the neighboring Mn magnetic ions [27], which are explained based on the Heusler alloy's magnetism [33]. Therefore, ^{119}Sn Mössbauer spectra would reflect the local magnetic field felt by the Sn atoms. As a result, the sextet or the magnetic component indicates the presence of a local magnetic field felt by the Sn atoms. Moreover, the singlet component can be attributed to Sn atoms with no transferred magnetic hyperfine field.

In the case of the ternary alloy $Ni_{50}Mn_{35}Sn_{15}$, with very close composition to that studied in this work, the presence of the singlet in the milled samples was ascribed to the presence of anti-phase boundaries (APB) induced during the milling process. The FM order is altered in the region of influence of APBs and in the stressed regions, in such a way that the total transferred dipolar field at Sn sites is zero, due to the AF coupling between Mn atoms in the APB. However, upon annealing, the AF coupling decreases and the FM coupling is restored as increasing the annealing temperature. As a result, the area of the sextet increases at the expense of that of the singlet, and the annealing of the singlet component directly reflects the relaxation of the internal stress, which is correlated with some MT features (e.g., transformation width). However, in the case of the quaternary $Ni_{45}Co_5Mn_{35}Sn_{15}$ alloy, also with very close composition to the one studied in this work, neutron diffraction performed at 10 K in the martensitic phase revealed AF coupling in both the milled and annealed samples. Even though the AF coupling decreases with annealing it does not become FM.

The Mössbauer spectra of the milled samples presented in this work reveal the characteristic singlet component related to the presence of APBs. After annealing at 873 K, the area of the singlet component diminishes in all spectra, even vanishing completely in most cases, see Figure 4. In the ternary alloy, and following the discussion of Ref. [16], the singlet component should vanish as a result of the elimination of the APBs upon annealing. However, as shown in Figure 4c, even in the milled state, the Sn13 sample does not exhibit the singlet component. The APBs induced during milling are still present as well as the AF coupling between the Mn atoms at 4*a* and 4*b* positions. However, there is no hint of the singlet component. The only difference between the milled and the annealed Sn13 (see Figure 4f) samples, is B_{hf} increase (from 6.54 T up to 7.8 T), which can be explained with the recovery of the FM coupling between 4*a* and 4*b* positions.

In this connection, a combined effect between the microstructural state, magnetic moments and Mn-Mn coupling may take place. As the measurement temperature decreases, the magnetism of the samples increases (see Figure 2). This fact implies that Mn atoms at 4*a* positions contribute with a greater magnetic moment to the overall magnetism as the FM coupling is reinforced. However, the singlet component reveals that at some Sn sites there is no transferred dipolar field. This could be due to the presence of regions where the atomic moments are randomly oriented, which on average result in an induced null transferred hyperfine field at Sn sites. In fact, Umetsu et al. [34] showed that in Ni-Mn-Sn systems the martensite may exhibit spin-glass magnetic behavior. As the temperature further decreases, the FM coupling between Mn moments may strengthen enough to induce a transferred hyperfine field in Sn nucleus which would explain the vanishing of the singlet component. However, further investigation is required to ascertain the exact mechanism.

On the other hand, in the case of $Ni_{45}Mn_{38}Sn_{13}Co_4$ alloy, the singlet component is clearly visible in all the milled samples, but this component is removed during the annealing. Taking into account that neutron measurements in similar quaternary alloys reveal AF coupling between 4*a* and 4*b* Mn positions in both milled and annealed samples, the singlet component should be present in the annealed martensite phase. However, as can be seen in Figure 4i,l, the singlet vanishes upon annealing. The behavior is very similar in the austenite phase, where the magnetic coupling is FM in both milled and annealed states, but nevertheless, the ^{119}Sn-MS spectra show a singlet contribution in the milled stated (FM coupling) and none in the annealed state (FM coupling). Therefore, the results shown in this work indicate that the cause of the lack of the total transferred dipolar field at Sn sites, is not only due to the AF coupling between Mn atoms in the close atomic environment of APBs. Due to this fact, in the Co-doped alloy, the stress-related singlet component can be resolved in the milled state in both martensite and austenite phases, see Figure 4g–i. Indeed, the singlet contribution revealed by ^{119}Sn-MS arises as a result of an intricate interplay between the microstructural state and the temperature dependence on the Mn-Mn coupling. As showed in the case of the ternary alloys studied in Ref. [16], the area of the singlet contribution does not disappear at the recovery temperature of

dislocations. It is still present above it up to temperatures 200 K higher, where the singlet area reaches 1%. In this region, the Mn-Mn coupling is FM and so, the singlet contribution must be mediated by the elimination of point defects, such as vacancies [35]. Therefore, the transferred dipolar field at Sn sites from the surrounding magnetic atoms depends very strongly on the microstructural order around Sn sites and on the stress field, which becomes ^{119}Sn-MS in a very powerful tool to study the microstructural stress in Sn containing metamagnetic shape memory alloys.

5. Conclusions

The effect of Co addition and the internal stresses are revealed at atomic level by ^{119}Sn-MS in $Ni_{50}Mn_{37}Sn_{13}$ and $Ni_{45}Mn_{38}Sn_{13}Co_4$ samples. The results show that M_s and B_{hf} follow the same temperature trend, concurrently with the evolution that the stress-related singlet component exhibits upon annealing. In $Ni_{45}Mn_{38}Sn_{13}Co_4$ alloy, the singlet can be tracked in a much wider range than in the ternary alloy, in both martensite and austenite phases. However, in the ternary alloy, this non-magnetic component can only be properly resolved within a limited temperature range, hindering the applicability of the approach reported in Ref. [16] for the $Ni_{50}Mn_{37}Sn_{13}$ sample. The fact that the temperature evolution of the singlet component in the ternary alloy cannot be explained only in terms of the Mn-Mn coupling, points out an intricate interplay between the microstructural state and the temperature dependence on the Mn-Mn coupling in Ni-Mn-Sn alloys.

Author Contributions: Conceptualization, I.U., J.A.G., J.S.G. and F.P.; software, J.A.R.-V., J.L.-G. and V.S.-A.; methodology, J.I.P.-L., V.S.-A. and J.A.R.-V.; formal analysis, I.U., J.L.-G., J.S.G., J.I.P.-L., V.S.-A. and J.A.R.-V.; investigation, I.U., J.L.-G., J.A.G. and J.S.G.; writing—original draft preparation, I.U., J.S.G., J.A.G. and F.P.; writing—review and editing, I.U., J.L.-G., J.A.R.-V., V.S.-A., V.R., J.A.G., J.I.P.-L., J.S.G. and F.P.; supervision, I.U., J.A.G., J.S.G. and F.P. All authors have read and agreed to the published version of the manuscript.

Funding: This research was funded by Projects RTI2018-094683-B-C5 (4,5) (MCIU/AEI/FEDER, UE) and Basque Government Grant IT-1005–16.

Conflicts of Interest: The authors declare no conflict of interest.

References

1. Yu, S.Y.; Liu, Z.H.; Liu, G.D.; Chen, J.L.; Cao, Z.X.; Wu, G.H.; Zhang, B.; Zhang, X.X. Large magnetoresistance in single-crystalline $Ni_{50}Mn_{50-x}In_x$ alloys ($x = 14 - 16$) upon martensitic transformation. *Appl. Phys. Lett.* **2006**, *89*, 162503. [CrossRef]
2. Planes, A.; Mañosa, L.; Acet, M. Magnetocaloric effect and its relation to shape-memory properties in ferromagnetic Heusler alloys. *J. Phys. Condens. Matter* **2009**, *21*, 233201. [CrossRef]
3. Sutou, Y.; Imano, Y.; Koeda, N.; Omori, T.; Kainuma, R.; Ishida, K.; Oikawa, K. Magnetic and martensitic transformations of Ni–Mn–X (X = In, Sn, Sb) ferromagnetic shape memory alloys. *Appl. Phys. Lett.* **2004**, *85*, 4358–4360. [CrossRef]
4. Kainuma, R.; Imano, Y.; Ito, W.; Sutou, Y.; Morito, H.; Okamoto, S.; Kitakami, O.; Oikawa, K.; Fujita, A.; Kanomata, T.; et al. Magnetic-field-induced shape recovery by reverse phase transformation. *Nature* **2006**, *439*, 957–960. [CrossRef] [PubMed]
5. Han, Z.D.; Wang, D.H.; Zhang, C.L.; Xuan, H.C.; Gu, B.X.; Du, Y.W. Low-field inverse magnetocaloric effect in $Ni_{50-x}Mn_{39+x}Sn_{11}$ Heusler alloys. *Appl. Phys. Lett.* **2007**, *90*, 042507. [CrossRef]
6. Krenke, T.; Duman, E.; Acet, M.; Wassermann, E.F.; Moya, X.; Manosa, L.; Planes, A. Inverse magnetocaloric effect in ferromagnetic Ni–Mn–Sn alloys. *Nat. Materi.* **2005**, *4*, 450–454. [CrossRef]
7. Liu, H.; Zhang, C.; Han, Z.; Xuan, H.; Wang, D.; Du, Y. The effect of Co doping on the magnetic entropy changes in $Ni_{44-x}Co_xMn_{45}Sn_{11}$ alloys. *J. Alloys Compd.* **2009**, *467*, 27–30. [CrossRef]
8. Liu, J.; Gottschall, T.; Skokov, K.P.; Moore, J.D.; Gutfleisch, O. Giant magnetocaloric effect driven by structural transitions. *Nat. Mater.* **2012**, *11*, 620–626. [CrossRef]
9. Sánchez-Alarcos, V.; Pérez-Landazábal, J.; Recarte, V.; Lucia, I.; Vélez, J.; Rodríguez-Velamazán, J. Effect of high-temperature quenching on the magnetostructural transformations and the long-range atomic order of Ni–Mn–Sn and Ni–Mn–Sb metamagnetic shape memory alloys. *Acta Mater.* **2013**, *61*, 4676–4682. [CrossRef]
10. Kumar, S.V.; Singh, R.; Raja, M.M.; Kumar, A.; Bysakh, S.; Mahendran, M. Microstructure and nanomechanical properties of Mn-rich Ni–Mn–Ga thin films. *Intermetallics* **2016**, *71*, 57–64. [CrossRef]
11. Pérez-Landazábal, J.I.; Sánchez-Alarcos, V.; Recarte, V.; Lambri, O.A.; Bonifacich, F.G.; Khanna, D.L.; Unzueta, I.; García, J.; Plazaola, F.; López-García, J.; et al. Influence of structural defects on the properties of metamagnetic shape memory alloys. *Metals* **2020**, *10*. [CrossRef]

12. Sánchez-Alarcos, V.; López-García, J.; Unzueta, I.; Pérez-Landazábal, J.; Recarte, V.; Beato-López, J.; García, J.; Plazaola, F.; Rodríguez-Velamazán, J. Magnetocaloric effect enhancement driven by intrinsic defects in a $Ni_{45}Co_5Mn_{35}Sn_{15}$ alloy. *J. Alloys Compd.* **2019**, *774*, 586–592. [CrossRef]
13. Sánchez-Alarcos, V.; Recarte, V.; Pérez-Landazábal, J.; Larumbe, S.; Caballero-Flores, R.; Unzueta, I.; García, J.; Plazaola, F.; Rodríguez-Velamazán, J. Mechanically induced disorder and crystallization process in Ni–Mn–In ball-milled alloys. *J. Alloys Compd.* **2016**, *689*, 983–991. [CrossRef]
14. Prasanna, A.A.; Ram, S. Local strains, calorimetry, and magnetoresistance in adaptive martensite transition in multiple nanostrips of $Ni_{39+x}Mn_{50}Sn_{11-x}$ ($x \leq 2$) alloys. *Sci. Technol. Adv. Mater.* **2013**, *14*, 015004. [CrossRef] [PubMed]
15. Alves, A.L.; Passamani, E.C.; Nascimento, V.P.; Takeuchi, A.Y.; Larica, C. Influence of grain refinement and induced crystal defects on the magnetic properties of $Ni_{50}Mn_{36}Sn_{14}$ Heusler alloy. *J. Phys. D Appl. Phys.* **2010**, *43*, 345001. [CrossRef]
16. Unzueta, I.; López-García, J.; Sánchez-Alarcos, V.; Recarte, V.; Pérez-Landazábal, J.I.; Rodríguez-Velamazán, J.A.; Garitaonandia, J.S.; García, J.A.; Plazaola, F. ^{119}Sn Mossbauer spectroscopy for assessing the local stress and defect state towards the tuning of Ni–Mn–Sn alloys. *Appl. Phys. Lett.* **2017**, *110*, 181908. [CrossRef]
17. Young, A.P.; Jakubovics, J.P. The effect of planar defects on exchange interactions in ferromagnetic metals. *J. Phys. F Metal Phys.* **1975**, *5*, 1866. [CrossRef]
18. Kamiyama, T.; Shinohara, T.; Tomiyoshi, S.; Minonishi, Y.; Yamamoto, H.; Asano, H.; Watanabe, N. Effect of deformation on Pd_2MnSn Heusler alloy studied with transmission electron microscopy, profile analysis of neutron powder diffraction pattern, and magnetization measurement. *J. Appl. Phys.* **1990**, *68*, 4741–4750. [CrossRef]
19. Caballero-Flores, R.; González-Legarreta, L.; Rosa, W.; Sánchez, T.; Prida, V.; Escoda, L.; Suñol, J.; Batdalov, A.; Aliev, A.; Koledov, V.; et al. Magnetocaloric effect, magnetostructural and magnetic phase transformations in $Ni_{50.3}Mn_{36.5}Sn_{13.2}$ Heusler alloy ribbons. *J. Alloys Compd.* **2015**, *629*, 332–342. [CrossRef]
20. Ma, S.; Cao, Q.; Xuan, H.; Zhang, C.; Shen, L.; Wang, D.; Du, Y. Magnetic and magnetocaloric properties in melt-spun and annealed $Ni_{42.7}Mn_{40.8}Co_{5.2}Sn_{11.3}$ ribbons. *J. Alloys Compd.* **2011**, *509*, 1111–1114. [CrossRef]
21. Brand, R.A. *Normos Mössbauer fit Program*; Laboratorium für Angewandte Physick: Duisburg, Germany, 1990.
22. Rodríguez-Carvajal, J. Recent advances in magnetic structure determination by neutron powder diffraction. *Phys. B Condens. Matter* **1993**, *192*, 55–69. [CrossRef]
23. Unzueta, I.; López-García, J.; Sánchez-Alarcos, V.; Recarte, V.; Pérez-Landazábal, J.I.; Rodríguez-Velamazán, J.A.; Garitaonandia, J.S.; García, J.A.; Plazaola, F. ^{119}Sn Mössbauer spectroscopy in the study of metamagnetic shape memory alloys. *Hyperfine Interact.* **2018**, *239*, 34. [CrossRef]
24. Sokolovskiy, V.V.; Buchelnikov, V.D.; Zagrebin, M.A.; Entel, P.; Sahoo, S.; Ogura, M. First-principles investigation of chemical and structural disorder in magnetic $Ni_2Mn_{1+x}Sn_{1-x}$ Heusler alloys. *Phys. Rev. B* **2012**, *86*, 134418. [CrossRef]
25. López-García, J.; Sánchez-Alarcos, V.; Recarte, V.; Rodríguez-Velamazán, J.; Unzueta, I.; García, J.; Plazaola, F.; La Roca, P.; Pérez-Landazábal, J. Effect of high-energy ball-milling on the magnetostructural properties of a Ni45Co5Mn35Sn15 alloy. *J. Alloys Compd.* **2021**, *858*, 158350. [CrossRef]
26. Passamani, E.C.; Córdova, C.; Alves, A.L.; Moscon, P.S.; Larica, C.; Takeuchi, A.Y.; Biondo, A. Magnetic studies of Fe-doped martensitic $Ni_2Mn_{1.44}Sn_{0.56}$-type Heusler alloy. *J. Phys. D Appl. Phys.* **2009**, *42*, 215006. [CrossRef]
27. Passamani, E.; Nascimento, V.; Larica, C.; Takeuchi, A.; Alves, A.; Proveti, J.; Pereira, M.; Fabris, J. The influence of chemical disorder enhancement on the martensitic transformation of the $Ni_{50}Mn_{36}Sn_{14}$ Heusler-type alloy. *J. Alloys Compd.* **2011**, *509*, 7826–7832. [CrossRef]
28. Umetsu, R.Y.; Sano, K.; Fukushima, K.; Kanomata, T.; Taniguchi, Y.; Amako, Y.; Kainuma, R. Mossbauer Spectroscopy Studies on Magnetic Properties for ^{57}Fe-substituted Ni-Mn-Sn Metamagnetic Shape Memory Alloys. *Metals* **2013**, *3*, 225–236. [CrossRef]
29. Kistner, O.C.; Sunyar, A.W. Evidence for quadrupole interaction of Fe^{57m}, and influence of chemical binding on nuclear gamma-ray energy. *Phys. Rev. Lett.* **1960**, *4*, 412–415. [CrossRef]
30. Shinohara, T.; Sasaki, K.; Yamauchi, H.; Watanabe, H.; Sekizawa, H.; Okada, T. On the reduction in magnetization by cold working on the ferromagnetic Heusler alloy Pd_2MnSn. *J. Phys. Soc. Jpn.* **1981**, *50*, 2904–2908. [CrossRef]
31. Ikeda, K.; Takahashi, S. Cold-working effect on magnetic properties in the Heusler alloys. *Phys. Rev. B* **1984**, *30*, 3808–3814. [CrossRef]
32. Takahashi, S.; Shinohara, T. Magnetic moment distribution in deformed Heusler alloy Pd_2MnSn. *J. Phys. F Metal Phys.* **1982**, *12*, 3115. [CrossRef]
33. Şaşıoğlu, E.; Sandratskii, L.M.; Bruno, P. First-principles calculation of the intersublattice exchange interactions and Curie temperatures of the full Heusler alloys Ni_2MnX ($X = Ga, In, Sn, Sb$). *Phys. Rev. B* **2004**, *70*, 024427. [CrossRef]
34. Umetsu, R.Y.; Kainuma, R.; Amako, Y.; Taniguchi, Y.; Kanomata, T.; Fukushima, K.; Fujita, A.; Oikawa, K.; Ishida, K. Mössbauer study on martensite phase in $Ni_{50}Mn_{36.5}{}^{57}Fe_{0.5}Sn_{13}$ metamagnetic shape memory alloy. *Appl. Phys. Lett.* **2008**, *93*, 042509. [CrossRef]
35. Unzueta, I.; de R-Lorente, D.A.; Cesari, E.; Sánchez-Alarcos, V.; Recarte, V.; Pérez-Landazábal, J.I.; García, J.A.; Plazaola, F. Experimental observation of vacancy-assisted martensitic transformation shift in Ni-Fe-Ga Alloys. *Phys. Rev. Lett.* **2019**, *122*, 165701. [CrossRef] [PubMed]